Proceedings of the
Annual Stability Conference
Structural Stability Research Council
Grapevine, Texas, April 18-21, 2012

Flexural and Axial Behaviour of CFRP Strengthened Steel Circular Hollow Section Beams and Short Columns

J. Haedir[1], X.-L. Zhao[2]

Abstract

The use of carbon fibre reinforced polymer (CFRP) sheets for strengthening steel hollow sections is a relatively new technique and provides advantageous of lightweight and strength enhancement. There are presently few applications that concern with composite strengthening of circular tubes with larger diameter-to-thickness ratios, and in the absence of clear theoretical understanding of behaviour to guide engineers, research is much needed to develop analytical and design models for such tubes strengthened by CFRP. This paper summarises a recent investigation at Monash University on the behaviour of circular hollow section (CHS) beams and short columns with varying section slenderness ratios and strengthened by CFRP sheets. Analytical models for determining the ultimate moment capacity and for predicting the moment-curvature response of CFRP-reinforced steel CHS beams are presented. The nonlinear model accounted for material properties of the steel and CFRP, volume fractions of the fibre and adhesive, amount of CFRP, and a wider range of section slenderness. The theoretical models were validated through comparisons with the test results. Design rules for predicting the strength of composite CHS under bending and compression were also proposed.

1. Introduction

The applications of high strength composite materials for strengthening of civil structures first began in the late 1980s (Hollaway 2003), followed by considerable research into the structural behaviour and failure modes of FRP-strengthened reinforced concrete (RC) members that showed strength enhancement (Hollaway and Leeming 1999, Hollaway 2008, 2010; Teng et al. 2002). In recent years, the problems related to ageing and structurally deteriorated steel structures, such as bridges, offshore platforms, communication towers and pipelines, have prompted resurgence in research and development of new materials for structural strengthening or repair. Strengthening with FRP may also be motivated by requirements of increased service loads and corrosion resistance, errors in the design, and insufficient maintenance. Replacing components of the existing structure is not an economic option. This addresses the need for cost-effective and structurally efficient strengthening techniques.

[1] PhD student, Dept. Civil Engineering, Monash University, <j.haedir@gmail.com>
[2] Professor, Dept. Civil Engineering, Monash University, <ZXL@monash.edu>

Research on combining FRP and steel in structural applications has made great strides and opened horizons for more efficient use of these materials (Moy 2001; Hollaway and Cadei 2002; Cadei et al. 2004; Jiao and Zhao 2004; Zhao and Zhang 2007, Zhao 2009). The structural engineers also have met the challenge to seek efficient and economical repair structural systems for various range and sections of steelwork going all the way to thin walled tubular sections. FRP materials possess high strength- and stiffness-to-weight ratios, corrosion resistance, and they can be tailored for specific applications. They are mainly composed of the reinforcing fibres embedded in polymeric resins. The polymer-based bonding substance regularly used for strengthening applications is an epoxy adhesive. The FRP composites may be attached to the tension flange of I-steel beams to provide additional flexural capacity (Miller et al. 2001; Sen et al. 2001; Moy and Nikoukar 2002; Tavakkolizadeh and Saadatmanesh 2003; Colombi and Poggi 2006) and improved fatigue life (Liu et al. 2009, 2010), or may be bonded to their thin webs to provide additional restraint against web buckling (Zhao and Al-Mahaidi 2009) and bearing failure (Zhao et al. 2006). The experimental investigations on the steel beams containing externally bonded FRP composites have shown that these systems are attractive as an option to conventional strengthening methods using bolting or welding of steel plates.

The alternative repair solution to the problems of ageing and structural deterioration may be extended to steel tubular structures which may be prone to local buckling (Shaat and Fam 2004, 2006a; Zhao and Zhang 2007, Seica et al. 2006, 2007; Bambach et al. 2009; Lanier et al. 2009). Steel tubular steel sections are widely used in engineering practice and in applications such as beams, columns, trusses, pedestrian bridges and recreational structures (Zhao and Hancock 2005). There are various types of loading on a tubular member, such as that imposed by its live loading, self-weight and wind loadings, which can result in conditions where the steel may yield, or buckle before reaching its yield limit. The local buckling is a form of instability which may occur in thin-walled members, and it relies upon the slenderness of the cross-section. It is understood that providing suitable constraints to minimise buckling deformations may ameliorate the buckling resistance. Hence, steel tubes with thin walls may be readily reinforced with FRP acting as an external constraint, to delay local buckling and to enhance the strength of tubes (Schnerch 2005; Photiou et al. 2006; Shaat and Fam 2006b, 2007, 2009; Teng and Hu 2007; Bambach and Elchalakani 2007; Nishino and Furukawa 2004).

Although previous work relating to the FRP strengthening of conventional steel members has been reported in recent years, limited studies have addressed the behaviour of steel tubular beams and short columns of wider section slenderness ratios wrapped with bi-directional carbon FRP sheets. In the absence of clear theoretical understanding of behaviour to guide engineers, research is much needed to develop analytical and design models for such tubes strengthened by CFRP. This paper summarizes an investigation carried out at Monash University on CHS externally strengthened using CFRP sheets and subjected to flexure and axial compression, which will provide an insight of the enhancement that CFRP will have on the strength and ductility. The strengthening degree of the CFRP directly depends on various factors, including the number of CFRP layers, strengthening configurations, fibre orientation, and volume fractions of the fibre and adhesives layers. Therefore, the analysis and design of reinforced steel tubular structures should account for these effects in practice.

2. Experimental Program

This section describes the experimental program, which included 18 CHS beams and 10 short columns made from cold-formed steel grade C350. All CHS beams were designed to encompass the limiting slenderness values for circular hollow sections, which in the Australian steel structures standard AS 4100 (Standards Australia 1998) were defined by compact, non-compact and slender sections. Four of the short columns were designed with the cross-section slenderness value exceeded the limit imposed in AS 4100. The normalized cross-section slenderness parameter (λ_s) for circular hollow sections under bending is usually expressed in the form

$$\lambda_s = \left(\frac{d^s}{t^s}\right)\left(\frac{\sigma_y^s}{250}\right) \tag{1}$$

in which σ_y^s is the yield stress of the steel and d^s/t^s is the ratio of the outer diameter of the steel to the wall thickness.

2.1 Tests specimens and materials

2.1.1 CHS beam specimens

Of all the beams were tested, five served as control bare steel specimens and the remaining beams were applied with CFRP sheets to the perimeter of the hollow steel core. The specimens were classified into three series depending on their cross-sectional sizes. Each series comprised of hollow and composite CFRP-steel CHS specimens with their respective diameter-to-thickness ratios. The measured geometric dimensions of the beam specimens are given in Haedir et al. (2009). Mean diameter and thickness values were determined through direct measurements. Series 1 and 2 consisted of beam sections, which were classified as compact and non-compact by current design rules, respectively. The remaining beam sections of Series 3 were considered to be slender. The differences between the composite specimens were the amount of CFRP, the orientation of CFRP and in how the bi-orientated fibres were asymmetrically distributed.

Each of the CHS beams had a span length (L) of 1500 mm and a machined length (L_m) of 800 mm. The ends of each machined specimen were internally stiffened with plaster, providing an effective length (L_f) of 400 mm, as shown in Fig. 1. The objective was to relieve the stress concentration beneath the loading points, thereby prohibiting local bearing failure of the CHS at lower stresses. Fig. 1 illustrates schematic diagrams of a reinforced test specimen and its cross-section with its fibre orientation layout.

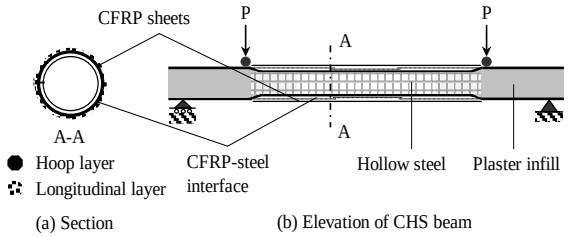

Figure 1: Schematic view of a CHS beam externally reinforced by CFRP reinforcement

2.2 Short columns

All steel columns were designed in order of increasing slenderness of the cross-section. The main parameters considered in this study included the local slenderness ratio (λ_s) which was in the range 67 to 142, the reinforcement ratio relative to steel (η) and the orientation of the reinforcing fibres with respect to the column axis. The measured properties of the specimens are given in Haedir and Zhao (2010). The test specimens were classified into four categories, in which columns of Series 3 and 4 were designed with the cross-section slenderness value greater than the limit imposed in the Australian steel structures code AS 4100. Each of the specimens was cut from a chosen tube size and then machined to obtain the required local slenderness value. The nominal length of each column was at least three times the outer diameter to obviate any effect on the strength due to column slenderness.

2.1.3 CFRP sheet and adhesives

The fibre reinforced polymer sheet material used for the tests was MBrace CF 130 high-strength carbon fibre with a sheet thickness of 0.176 mm. The carbon fibre sheets were bonded around the CHS perimeter using a high-performance two-part (Araldite Part A/B) room temperature cure epoxy adhesive. Preparation of epoxy adhesive entails the mixing of epoxy resin (Part A) with a chemical catalyst (Part B) in a 5:2 weight ratio. The two-part adhesive had a pot life of 1 hour under ambient temperature (25^{o}C). The mechanical properties of the CFRP (CF 130) and two-part epoxy adhesive were determined by Fawzia (2007) and were used in this study. The average CFRP tensile strength and elastic modulus are 2675 and 230 MPa, respectively. The mean adhesive tensile strength and elastic modulus are 28.6 and 1901 MPa, respectively, with a Poisson's ratio of 0.36.

2.2 Test procedures

2.2.1 Preparation of specimens

Prior to attachment of the reinforcing carbon fibre sheets to the steel CHS, the surface of the steel was ground with an abrasive disc and then solvent cleaned to obviate any contamination of the surface and to promote good adhesion. Each layer of CFRP was prepared according to the required dimensions, and the mixed epoxy was smeared uniformly on the surface of the fibre sheet. The CFRP sheets contained orthogonally orientated reinforcing fibre layers - *hoop* fibre reinforcing sheets with layers orientated perpendicularly to the length axis of the beam (Fig. 2a), allowing the fibres to exert a circumferential restraint on the buckling tendency of the compression steel wall, and *longitudinal* fibre reinforcing sheets having layers orientated parallel to the length axis (Fig. 2b), promoting the contribution of the tension regions to the bending strength of the steel tube. For each layer of CFRP attached, the vertical and horizontal diameters of the composite section, d_v^c and d_h^s, were measured. The wrapped composite sheet was then gradually pressed along the fibre axis with a paddle roller to ensure a uniform bond thickness. At the adjacent end of the column specimen, a length of 12.5 mm was unreinforced to accommodate the possible loading of the CFRP-reinforced column solely on the steel, shown in Fig. 3(b).

(a) Orientation of *hoop* (H) fibre sheet (b) Orientation of *longitudinal* (L) fibre sheet

Figure 2: Orientation of CFRP sheets

2.3 Test set-up and instrumentation

The beams were tested with a four-point loading system as a means of inducing a state of pure bending. A photograph of a typical specimen (CF-SL1A) in the test rig at the commencement of testing is given in Fig. 3a. The loads were applied through a hand operated hydraulic pump that extends to two hydraulic jacks. The tubes were instrumented with longitudinal strain gauges on the compression and tension faces of the tube at the mid-length. Two magnetic inclinometers were placed on the left and right sides of the specimen to monitor the angle of rotations.

The instrumentation in the short column tests included string potentiometers and linear electric resistance strain gauges. A total of three string pots were placed between a pair of parallel end plates to determine the axial shortening of the test columns. Fig. 3b gives a schematic location of the string pots. Steel end plates were used in the columns to provide a uniform distribution of bearing stresses to the column. Each plate had a circular recessed centre which was filled with a small amount of rigid plaster before mounting them to the column ends.

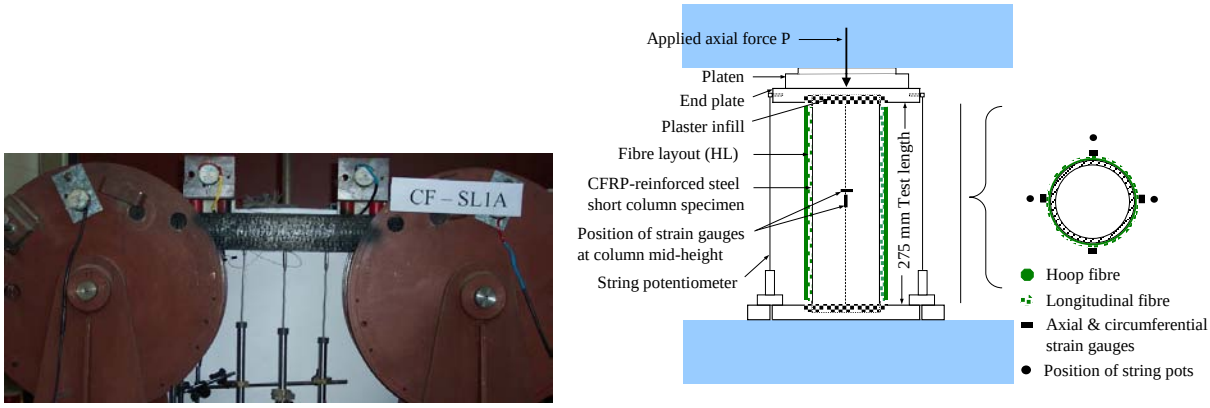

(a) Flexure (b) Compression

Figure 3: Apparatuses for flexural and compression tests of CHS

2.4 Experimental results

2.4.1 Moment-rotation curves

The moment-rotation behaviour of a composite beam is a useful measure of the parameters reflecting the stiffness, strength and rotation capacity of the beam. Figs. 4(a)-(d) provides the measured moment-rotation curves for the beams of Series 1-3. The plotted rotations represent the angles measured from one side of the specimen. The beams of Series 1 were each designed to reach its sectional plastic moment capacity (M_p^s). The same fibre orientation layout as in composite beams of Series 2 was used for the two composite specimens in Series 1, whilst one specimen was tested as a bare steel member. It can be seen in Fig. 4(a) that the addition of CFRP increases the bending strength slightly above the plastic moment capacity of the steel. Specimens CF-NC1A and CF-NC1B with the inclusion of fibre sheet reinforcing were able to achieve 15 and 23% higher than the sectional plastic moment capacity calculated for the untreated steel section (Fig. 5(b)). It can be seen from the figure that in the advanced stages of loading particularly after attainment of the ultimate load, the behaviour for reinforced section CF-NC1A is characterised by a noticeable diminution in the moment resistance followed by a sustained load near M_p^s until failure occurred. The drop in load was attributed to the rupture of the CFRP on the compression side of the tube and occurred after yielding of the steel tube.

The moment-rotation response of specimen CF-SL2C reinforced with only one layer of longitudinal CFRP is shown in Fig. 4(d). It can be seen that as the ultimate load is reached, the moment decreases sharply compared with the other reinforced specimens in Series b. Collapse of the tube wall occurred beyond this point. In the case of the beams with slender sections in Figs. 4(c)-(e), the variation in the rotation response for the beams with a minimum of two fibre layers is evident, and the reinforced sections reach or exceed the plastic moment strength (M_p^s) and exhibit higher rotations than the bare steel specimens. The attainment of the plastic moment would suggest that the compactness of the section is, in effect, influenced by the contribution of reinforcing fibres. Buckling was delayed by the addition of the hoop CFRP sheets, as compared with the tests that did not have any hoop CFRP sheets. It can also be seen in Fig. 4(d) that the ductility and stiffness of these beams are also enhanced.

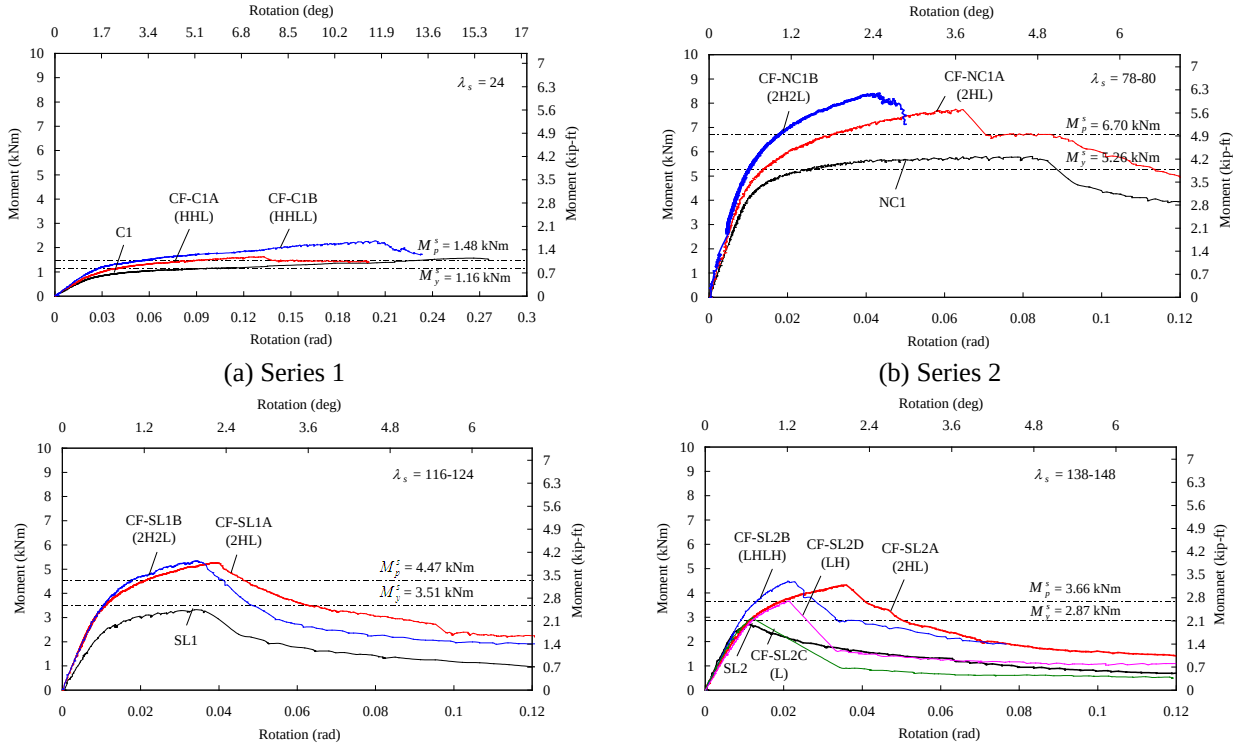

(a) Series 1 (b) Series 2

(c) Series 3a (d) Series 3b

Figure 4: Moment-rotation curves of CHS beams

2.4.2 Axial-load shortening curves

Typical examples of the axial load-shortening characteristics for the columns tested are shown in Figs. 5(a)-(b), which provide useful comparisons of the performance of equivalent steel sections with and without fibre reinforcement. The average axial shortening was recorded from the three string pots. The curves demonstrate the influence on the axial shortening as the percentage of fibre reinforcement increases in the composite sections. The reinforced section columns exhibited different post-yield characteristics relative to the amount of CFRP reinforcement used. The curves in the figure depict the post-elastic loads of reinforced sections, which are above that of steel only. It may be seen from these curves that, in general, for reinforced specimens, the initial buckle appeared to occur when the axial load had reached its maximum value, and this behaviour is shown by the descending branch of the load-shortening response.

For the case of sections with higher values of local slenderness ratio of the steel tube, it is exemplified in Figs. 5(c) how the reinforcing effect of the composite fibres also enhances the axial capacities of slender sections. All the composite slender section specimens present consistent axial shortening at ultimate load with the bare steel counterpart, indicating no significant loss of axial rigidity prior to failure.

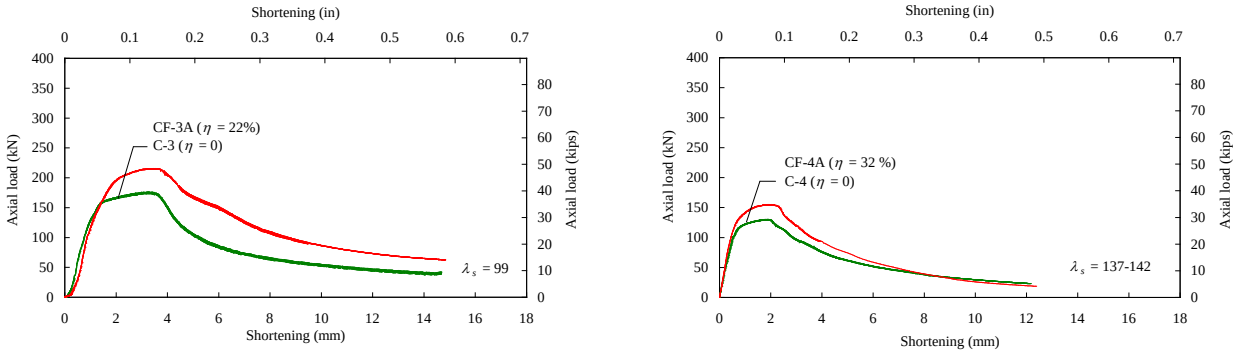

(a) λ_s = 99 (b) λ_s = 137-142

Figure 5: Axial load-shortening curves of short bare steel and reinforced columns

2.4.3 Ultimate flexural and compressive strength

The measured ultimate bending moments for all the beams tested are presented in Table 1; the table also gives the corresponding ratios of the ultimate moments of the reinforced specimens (M_u^{cs}) relative to the bare steel specimens (M_u^s) and the design plastic moment capacity (M_p^s) of

Table 1: Flexural strength of tested beams

Test Series	Specimen No.	σ_y^s (N/mm^2)	λ_s	Fibre Orientation Layout	M_p^s (kNm)	M_u (kNm)	$\frac{M_u^{cs}}{M_u^s}$
1	C1	479	24.0	-	1.48	1.55	-
	CF-C1A	479	24.2	HHL	1.46	1.60	1.03
	CF-C1B	479	24.0	HHLL	1.48	2.24	1.45
2	NC1	455	80.0	-	6.70	5.80	-
	CF-NC1A	455	79.1	HHL	6.78	7.77	1.34
	CF-NC1B	455	78.0	HHLL	6.88	8.45	1.46
3	SL1	470	122.1	-	4.47	3.32	-
	CF-SL1A	470	116.5	HHL	4.71	5.24	1.58
	CF-SL1B	470	124.1	HHLL	4.37	5.30	1.60
	SL2	457	139.1	-	3.66	2.69	-
	CF-SL2A	457	138.3	HHL	3.68	4.32	1.60
	CF-SL2B	457	138.7	LHLH	3.65	4.48	1.67
	CF-SL2C	468	147.8	L	3.61	2.98	1.11
	CF-SL2D	468	141.2	LH	3.78	3.66	1.36
	SL3	457	163.9	-	3.07	2.13	-
	CF-SL3A	468	180.1	HHHL	2.92	3.23	1.52
	CF-SL3B	468	172.1	HLHL	3.06	4.08	1.92
	CF-SL3C	470	179.2	HHLL	2.95	3.91	1.84

the steel section. The results elucidate the role the CFRP reinforcement plays in augmenting the strength through the effective exploitation of the longitudinal fibre strength and the restraining action of the hoop-orientated fibres. Furthermore, the ultimate compressive loads of the columns are summarised in Table 2, together with the corresponding yield strength of the bare steel section (N_y^s).The strength gains in reinforced specimens with section slenderness ratios greater than 80 were also compared against their bare steel counterparts. The non-dimensionalised ratios of the experimental load with respect to the yield strength of the steel column provide a measure of the effective contribution CFRP makes to improve the local buckling resistance of the steel tube.

Table 2: Compressive strength of tested columns

Specimen No.	d^s mm	t^s mm	σ_y^s N/mm^2	$\frac{L}{d^s}$	$\frac{d^s}{t^s}$	λ_s	N_y^s kN	N_{exp} kN	$\frac{N_{exp}}{N_y^s}$
CF-1A	87.23	2.32	455	3.2	38	68	282	299	1.06
CF-1B	87.21	2.32	455	3.2	38	68	281	341	1.21
C-2	86.31	2.00	455	3.2	43	79	241	217	0.90
CF-2A	86.38	1.91	455	3.2	45	82	230	267	1.16
CF-2B	86.39	1.96	455	3.2	44	80	236	281	1.19
C-3	85.75	1.57	455	3.2	55	99	189	176	0.93
CF-3A	85.68	1.57	455	3.2	54	99	189	214	1.13
C-4	85.11	1.13	455	3.2	75	137	136	130	0.96
CF-4A	85.21	1.10	455	3.2	78	142	132	155	1.18

2.4.4 Failure modes

Typical local failure modes of the tested specimens are exhibited in Figs 6(a)-(f). In general, for the composite CFRP-steel sections, the failure was precipitated by local collapse of the section in the compression zone, with buckling of the steel wall and/or crushing of the CFRP evident. After testing, reinforced sections CF-NC1A and CF-SL2A were saw-cut at the mid-span region to observe the failure mode of the cross-section. Figs. 6(c)-(d) show a close-up of the compressed zone for the beam, illustrating the extent of the localised failure in the composite CHS section. Local CFRP crushing was found at locations corresponding to local inward bulges of the outer tubes. Debonding of the CFRP-steel interface did not typically occur, with the exception being CF-NC1B.

(a) CF-C1B

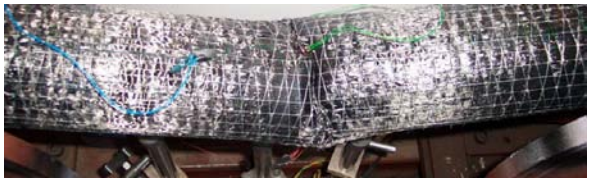

(b) CF-SL1A

(c) CF-NC1A

(d) CF-SL2A

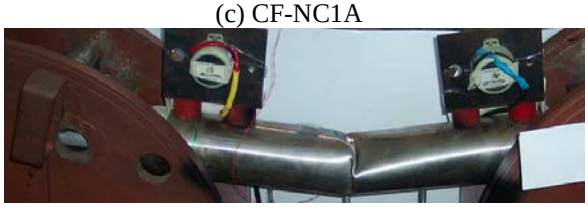

(e) SL3

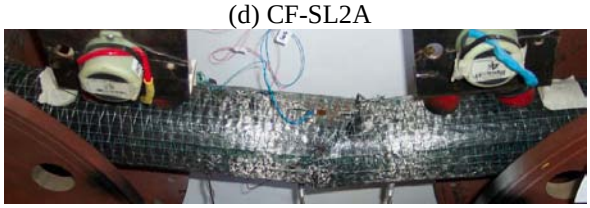

(f) CF-SL3C

Figure 6: Failure modes of CHS beams

The typical failure modes of tested columns are shown in Figs 7(a)-(j). In unreinforced column C-1 with a low slenderness ratio of 68, the usual bellow type of buckling was observed near the ultimate load, whilst inwards local bulging after one or more buckles governed the failure mode of bare steel specimens C-3 and C-4 with higher section slenderness, as indicated in Figs. 8(g) and (i). For reinforced column CF-1A with 1H1L fibre layout, outward buckling near the column end was observed at failure (Fig. 7(b)). This is illustrated by a load drop after the column reached its ultimate load. In specimen CF-1B of Series 1 reinforced with additional CFRP layers orientated in both the hoop and longitudinal directions, inward bulges were also observed at mid-length of the tube, as shown in Fig. 7(c). The mean CFRP strain at which the section reached its peak load was 1138 $\mu\varepsilon$.

Local damage was evident in reinforced column CF-2B with 2L2H fibre layout. The outer hoop fibres showed insufficient restraining force to inhibit outward buckling near the end regions of the column, leading to fibre rupture (Fig. 7f). This behaviour was attributed to cracks emanating from the fibre-adhesive interface. For specimen CF-3A with a slenderness ratio of 99 and

(a) C-1

(b) CF-1A

(c) CF-1B

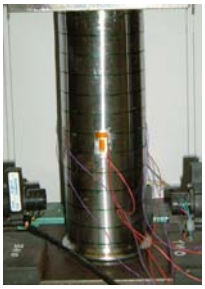

(d) C-2

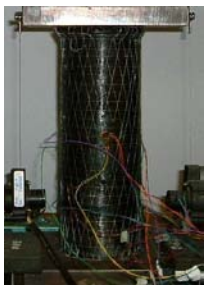

(e) CF-2A

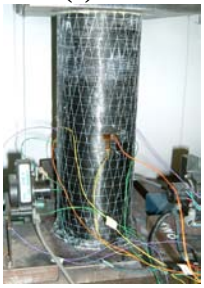

(f) CF-2B

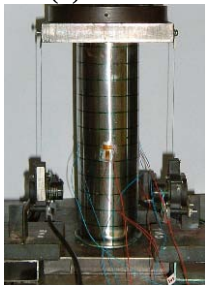

(g) C-3

(h) CF-3A

(i) C-4

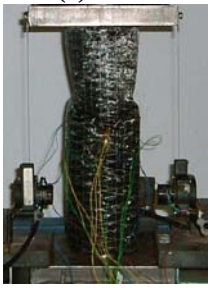

(j) CF-4A

Figure 7: Failure modes of columns

strengthened with 1H1L fibre layers, crushing of CFRP sheets was observed at one-third height of the tube, as revealed in Fig. 7(h). Crushing of CFRP occurred when the steel wall bulged inwards, likely after reaching the peak load. Following the inward buckling of the tube, the stiffness continued to decrease due to further crushing of the CFRP in compression. Similarly, the mechanism of failure for reinforced column CF-4A with higher section slenderness ratio and the same number of fibre layers is inward buckling of the strengthened steel, as shown in Fig. 7(j). The ultimate capacity of 155 kN was reached just before the onset of local buckling, and this value was above the strength of the bare steel tube. Further loading after buckling resulted in a gradual reduction in strength. This behaviour indicates how effective the CFRP sheets are in delaying the steel skin buckling locally. The average strain in the fibre at ultimate was 2375 $\mu\varepsilon$. This value is slightly above the yield strain of steel obtained from coupon tests. No debonding of CFRP was observed in all the tests.

3. Ultimate Strength Analysis of CFRP-Strengthened Steel CHS Beams

A typical FRP-externally reinforced steel composite CHS beam is made of CFRP layers and a hollow steel beam, as shown in Fig. 8. The accuracy of the analytical predictions depends mainly upon how suitable the conditions provide the actual capacity of the cross-section. The composite cross-section area domain is composed of the carbon FRP, denoted as A^{cs}, and the steel component, denoted as A^{s}.

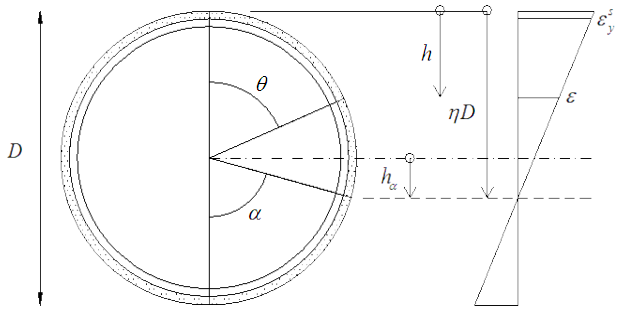

Figure 8: Composite cross-section and strain diagram

In the analysis of the composite beam, it is assumed that plane sections remain plane after bending. The composite cross-section is assumed to be symmetrical with respect to the axis of bending. Perfect bond is also assumed to exist between the steel and the CFRP and that strains are linearly distributed throughout the depth. Also, the steel is assumed to be either elastic-plastic or elastic with negligible strain hardening. For simplicity considerations, it is assumed that the constitutive relations in both tension and compression for steel to be the same. The hoop fibres in compression are considered in the section. With the linear strain profile represented by initial yielding of the steel at the top compression fibre (ε_y^s), the strain at a desired point across the depth of the composite cross-section is then calculated. By using the stress-strain characteristics of cold-formed steel and carbon FRP, the desired stress is then evaluated.

The resultant of the internal forces is found by integrating the internal stress in the section over the area, as generally expressed in Eq. (2). The requirement is used to adjust the angle of rotation (θ) in which dA^i is dependent upon, corresponding to the neutral axis depth, $h_n = \eta D$, in which η is the position of the neutral axis depth and D is the diameter of the composite section, as

indicated in Fig. 8. Generally, if the compressive forces exceed the tensile forces, then h_n has to be reduced in the subsequent iteration. Once horizontal equilibrium is reached, the internal moment M resisted by the composite cross-section is determined as

$$\int_{A^i} \sigma(\varepsilon)\, dA^i = P \tag{2}$$

$$\int_{A^i} \sigma(\varepsilon) R^i \cos\theta\, dA^i = M \tag{3}$$

where $P = 0$ is the loading condition for a member due to pure bending, A^i is the cross-sectional area of the respective components (i.e. the steel and the CFRP layers), $\sigma(\varepsilon)$ is the stress in the material as a function of its strain, and R^i represents the radius of the respective components.

3.1 Composite section with longitudinal fibre layers under an elastic only condition

The cross-sectional geometries used in this analysis are derived from the tested beam sections. The assumption for analysis of the tubular composite section is that the behaviour of the FRP-steel in both the compression and tension zones is considered elastic. The strain distribution is depicted in Fig. 9.

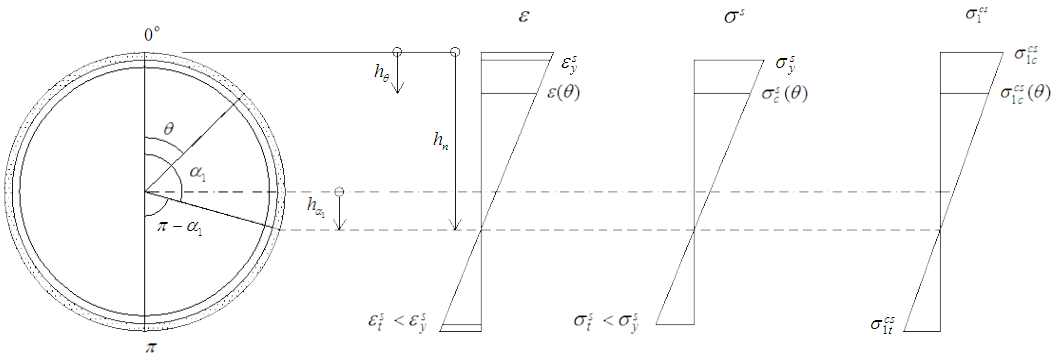

Figure 9: Strain and stress distributions under an elastic only condition

The maximum compressive and tensile strains in the top and bottom fibres of the steel section is defined by ε_y^s. The strain at any location in the cross-section can be determined with reference to the above strain distribution. The resultant force ΣP can be calculated by enforcing equilibrium of all horizontal forces of the section, which is given by

$$\sum P = P^s + P^{cs} = 0 \tag{4}$$

where P^s and P^{cs} correspond to the internal forces of the steel and the CFRP, respectively. Complete derivations of the equations are given in Haedir et al. (2010). Taking advantage of the cross-sectional symmetry, the force in the steel can be written as

$$P^s = \frac{2\sigma_y^s R^s t^s}{R^s + h_{\alpha_1}}\left(h_{\alpha_1}\pi\right) \tag{5}$$

As for the CFRP, two approaches are considered in this analysis, one that takes into account the CFRP in compression and tension, and the other that disregards the CFRP in compression. These approaches are represented, respectively, as

$$P^{cs} = \frac{2\sigma_{1c}^{cs} R^{cs1} t^{cs1}}{R^{cs1} + h_{\alpha_1}} \left(R^{cs1} \sin\alpha_1 + h_{\alpha 1} \alpha_1 \right) - \frac{2\sigma_{1t}^{cs} R^{cs1} t^{cs1}}{R^{cs1} - h_{\alpha_1}} \left(- h_{\alpha_1} \pi + R^{cs1} \sin\alpha_1 + h_{\alpha_1} \alpha_1 \right) \tag{6}$$

$$P^{cs} = - \frac{2\sigma_{1t}^{cs} R^{cs1} t^{cs}}{R^{cs1} - h_{\alpha_1}} \left(- h_{\alpha_1} \pi + R^{cs1} \sin\alpha_1 + h_{\alpha_1} \alpha_1 \right) \tag{7}$$

When the number of carbon fibre layers is in the range of $1 \le n \le 4$, the force in the carbon fibre section can be written in general form as

$$P^{cs} = \sum_{n=1}^{j} \frac{2\sigma_{1c}^{cs} R^{csn} t^{csn}}{R^{csn} + h_{\alpha_1}} \left(R^{csn} \sin\alpha_1 + h_{\alpha_1} \alpha_1 \right) - \frac{2\sigma_{1t}^{cs} R^{csn} t^{csn}}{R^{csn} - h_{\alpha_1}} \left(- h_{\alpha_1} \pi + R^{csn} \sin\alpha_1 + h_{\alpha_1} \alpha_1 \right) \tag{8}$$

The neutral axis rotation angle α_1 can be obtained from equilibrium of forces. Subsequently, the expression for the ultimate moment M can be found by the summation of all forces of the section with respect to its neutral axis, where the internal steel moment can calculated by

$$M^{s} = \frac{2\sigma_{y}^{s} \left(R^{s} \right)^2 t^{s}}{R^{s} + h_{\alpha_1}} \left(\frac{R^{s} \pi}{2} \right) \tag{9}$$

and the bending moment resulting from the CFRP, taking into account the compressive and tensile forces, can be determined as

$$\begin{aligned} M^{cs} = & \frac{2\sigma_{1c}^{cs} \left(R^{cs1} \right)^2 t^{cs1}}{R^{cs1} + h_{\alpha_1}} \left(\frac{R^{cs1} \sin\alpha_1 \cos\alpha_1}{2} + \frac{R^{cs1} \alpha_1}{2} + h_{\alpha_1} \sin\alpha_1 \right) \\ & - \frac{2\sigma_{1t}^{cs} \left(R^{cs1} \right)^2 t^{cs1}}{R^{cs1} - h_{\alpha_1}} \left(- \frac{R^{cs1} \pi}{2} + \frac{R^{cs1} \sin\alpha_1 \cos\alpha_1}{2} + \frac{R^{cs1} \alpha_1}{2} + h_{\alpha_1} \sin\alpha_1 \right) \end{aligned} \tag{10}$$

In the case when only the tensile zone of CFRP is considered, the moment capacity of the CFRP can be calculated as

$$M^{cs} = - \frac{2\sigma_{1t}^{cs} \left(R^{cs1} \right)^2 t^{cs1}}{R^{cs1} - h_{\alpha_1}} \left(- \frac{R^{cs1} \pi}{2} + \frac{R^{cs1} \sin\alpha_1 \cos\alpha_1}{2} + \frac{R^{cs1} \alpha_1}{2} + h_{\alpha_1} \sin\alpha_1 \right) \tag{11}$$

In general, when the number of carbon fibre layers is increased to $1 \le n \le 4$, the resulting moment equation for the CFRP can be written in the form

$$M^{cs} = \sum_{n=1}^{j} \frac{2\sigma_{1c}^{cs}\left(R^{csn}\right)^2 t^{csn}}{R^{csn}+h_{\alpha_1}}\left(\frac{R^{csn}\sin\alpha_1\cos\alpha_1}{2}+\frac{R^{csn}\alpha_1}{2}+h_{\alpha_1}\sin\alpha_1\right) - \sum_{n=1}^{j} \frac{2\sigma_{1t}^{cs}\left(R^{csn}\right)^2 t^{csn}}{R^{csn}-h_{\alpha_1}}\left(-\frac{R^{csn}\pi}{2}+\frac{R^{csn}\sin\alpha_1\cos\alpha_1}{2}+\frac{R^{csn}\alpha_1}{2}+h_{\alpha_1}\sin\alpha_1\right) \tag{12}$$

4. Moment-Curvature Analysis

In this section, a cross-sectional nonlinear analysis used for predicting the moment-curvature and moment-strain responses of a CHS beam strengthened with CFRP sheets is presented. The method used in this thesis requires the derivation of equilibrium equations, in which their solutions are obtained using the incremental-iterative technique. The associated derivation of the tangent stiffness matrix was also given. The stiffness-based approach used by Ghali and Favre (1994) and Bradford and Gilbert (1989) in their study of the time-dependent behaviour of conventional concrete and steel-concrete composite beams, will also be used here. The nonlinear analysis accounts the contribution of the strengthening system to the enhancement of the flexural behaviour of the circular steel tube wrapped with bonded CFRP sheets. The solution is obtained for the case of a CHS beam strengthened by CFRP sheets mainly in the longitudinal and hoop directions. The amount of CFRP reinforcement, different strengthening configurations, fibre and adhesive volume fractions and material non-linearity are considered herein.

The material models for composite materials such as those given in Jones (1999) and Kaw (2006) were used in this analysis, and further illustrations can be found in Haedir et al. (2011). In the present study, a trilinear model for the stress-strain relationship of the steel layers is adopted in the non-linear sectional analysis. The stress in various parts of the curve is defined as follows:

$$\sigma = \begin{cases} E^s\varepsilon & \text{for } \varepsilon \le \sigma_{pt}^s / E^s \\ \sigma^s & \text{for } \varepsilon_{pt}^s < \varepsilon < \varepsilon_1 \\ \sigma_{yt}^s & \text{for } \varepsilon \ge \varepsilon_1 \end{cases} \tag{13}$$

in which E^s is the steel elastic modulus, ε is the strain in the steel, σ^s is the stress in the steel and is represented as

$$\sigma^s = \left(\frac{\sigma_{yt}^s - \sigma_{pt}^s}{\varepsilon_y^s - \sigma_{pt}^s / E^s}\right)\left(\varepsilon - \varepsilon_{pt}^s\right) + \sigma_{pt}^s \tag{14}$$

and σ_{yt}^s is the tensile yield stress, and where the proportional limit of the steel σ_{pt}^s is taken to be 0.75 of the steel yield stress. The strain ε_1 at which the stress reaches σ_{yt}^s is taken as 0.0045. The tensile yield stress σ_{yt}^s and strain ε_y^s were determined from a coupon test as 450 N/mm^2 and 2250 $\mu\varepsilon$, respectively.

4.1Strain and stress distribution

The cross-section is assumed to be symmetrical about a vertical axis and the strain distribution is assumed to be linear. The cross-section is assumed to remain plane after deformation. A typical strain profile over the cross-section is adopted as shown in Fig. 10. The reference axis is taken from the top fibre, and the strain at any point below the top fibre of the section can be determined with respect to the curvature.

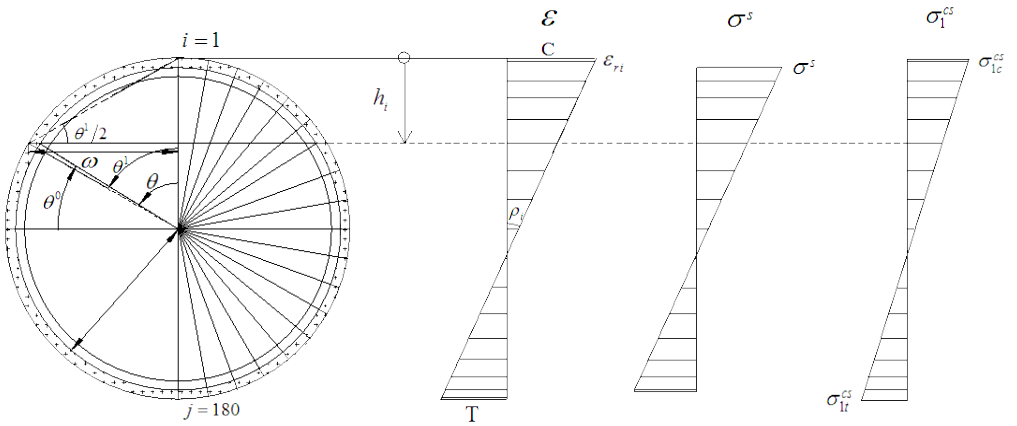

Figure 10: Strain and stress distributions in a CFRP-reinforced steel composite CHS section

The strain in the fibre induces a moment M and P in the cross-section. By dividing the section into angular points (j = 180) and translating them into their corresponding h-coordinates, the load components M and P can be obtained by integrating over each fibre of the cross-section and then employing the trapezoidal integration method resulting in

$$\begin{bmatrix} P \\ M \end{bmatrix} = \begin{bmatrix} \sum_{i=1}^{j} E_i^{c1}(\varepsilon)\int_A dA + \sum_{i=1}^{j} E_i^{s}(\varepsilon)\int_A dA & -\sum_{i=1}^{j} E_i^{c1}(\varepsilon)\int_A h_i dA - \sum_{i=1}^{j} E_i^{s}(\varepsilon)\int_A h_i dA \\ -\sum_{i=1}^{j} E_i^{c1}(\varepsilon)\int_A h_i dA - \sum_{i=1}^{j} E_i^{s}(\varepsilon)\int_A h_i dA & \sum_{i=1}^{j} E_i^{c1}(\varepsilon)\int_A h_i^2 dA + \sum_{i=1}^{j} E_i^{s}(\varepsilon)\int_A h_i^2 dA \end{bmatrix} \begin{bmatrix} \varepsilon_{ri} \\ \rho_i \end{bmatrix} \tag{15}$$

in which $E_i^{c1}(\varepsilon)$ and $E_i^{s}(\varepsilon)$ are Young's moduli of the composite fibres and steel, respectively, determined according to their material characteristics (Haedir et al. 2011). It is to be noted that Eqs. (15) has to include the symmetrical component of the circular section. Eq. (15) can be expressed as

$$[F] = [K(\varepsilon)][\upsilon]_i \tag{16}$$

where $[F]$ is the force matrix, $[K(\varepsilon)]$ is the tangent stiffness matrix and $[\upsilon]_i$ is the corresponding deformation matrix. With known values of externally applied forces M and P, the above equation can be solved for $[\upsilon]_i$ that contains the strain ε_{ri} at the reference level and the curvature ρ_i component.

4.2 Comparison of moment-curvature results

The moment-curvature curves for the FRP-strengthened steel CHS beams tested in this study are shown in Figs. 11(a)-(d), together with the theoretical curves. The graphs are plotted in a non-dimensional format, i.e., $M_{reinforced}/M_{steel}$ versus ρreinforced/ρsteel, where $M_{reinforced}$ and $\rho_{reinforced}$ are the moment and curvature for the CFRP reinforced CHS beams, respectively, and M_{steel} and ρ_{steel} are those for bare CHS beams. The value of M_{steel} is given in Haedir et al. (2009), whereas ρ_{steel} is defined as $M_{steel}/(EI)_{steel}$. Failure is assumed to occur prior to the longitudinal CFRP reaching its ultimate strain. The behaviour is initially linear in each case. After first yielding of the steel in compression occurs in the outer section, the behaviour becomes non-linear as the CFRP crushes in compression and steel yielding progresses towards the tension wall. It is shown from these figures that the model developed in this study is capable of tracing the initial stiffness behaviour of the test specimens.

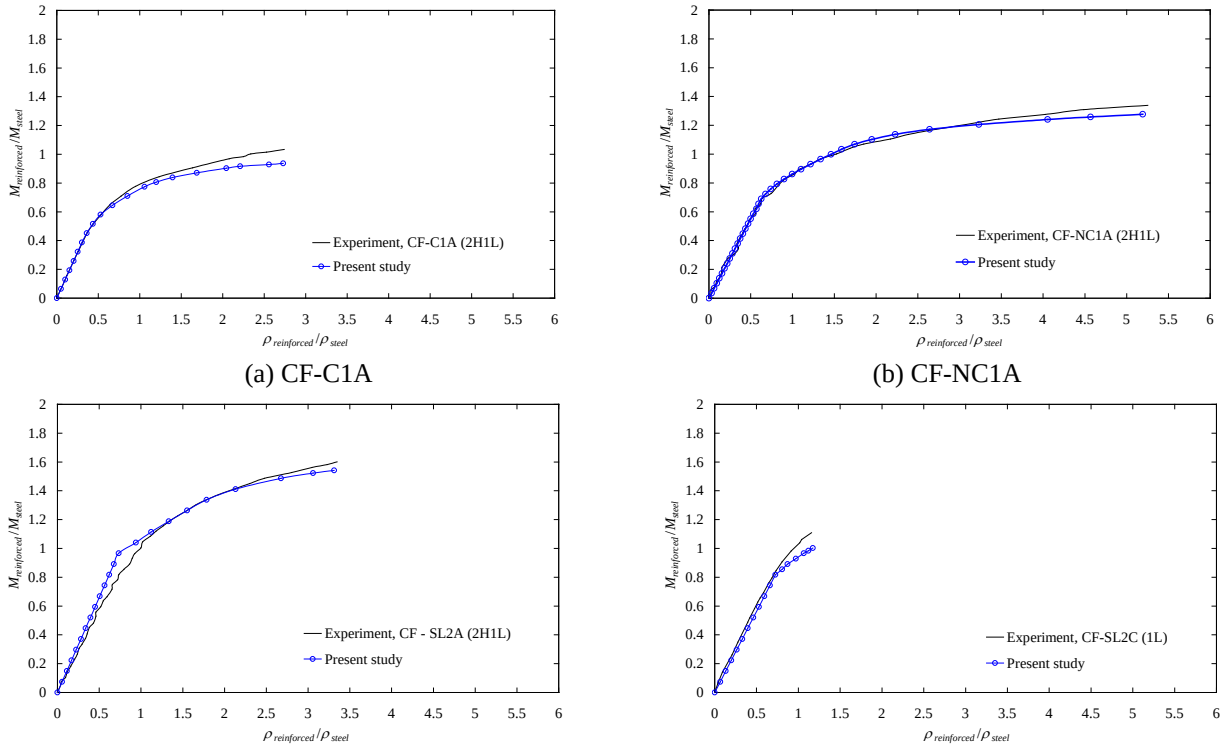

(a) CF-C1A (b) CF-NC1A

(c) CF-SL2A (d) CF-SL2C

Figure 11: Moment-curvature curves of reinforced steel CHS beams

5 Design rules for CFRP reinforced-steel tubular beams subjected to bending

5.1 Proposed method of design

The thickness of the supplanted area from CFRP to steel is calculated as

$$t_{es}^{cs} = n_L \beta_L t_L^{cs} + n_H \beta_H t_H^{cs} \tag{17}$$

in which n_L and n_H are the number of longitudinal and hoop CFRP sheets, respectively, t_L^{cs} and t_H^{cs} are the thicknesses of longitudinal and hoop carbon fibre sheets, respectively, and β_L is the modular ratio associated to the longitudinal fibres, given as

$$\beta_L = E_{1t}^{cs} / E^s = E_{1c}^{cs} / E^s > 1.0 \tag{18}$$

and β_H is the modular ratio related to the hoop fibres, which is defined as

$$\beta_H = E_{2t}^{cs} / E^s = E_{2c}^{cs} / E^s < 1.0 \tag{19}$$

in which E_{1t}^{cs} and E_{1c}^{cs} are Young's moduli of longitudinal carbon fibres in tension and in compression, respectively, E_{2t}^{cs} and E_{2c}^{cs} are Young's moduli of hoop carbon fibres in tension and in compression, respectively. It is assumed in Eq. (18) that the longitudinal CFRP has the same modulus of elasticity in tension and compression. Likewise, in Eq. (19), it is assumed for the hoop CFRP that the modulus of elasticity is the same in tension as in compression.

The elastic modulus of the hoop CFRP is transformed into an equivalent elastic modulus of the longitudinal carbon fibres by applying a proportioning factor (ξ), as shown below

$$\beta_H = E_{2t}^{cs} / E^s = \xi E_{1t}^{cs} / E^s = \xi \beta_L \quad \text{for } 0 \le \xi \le 0.80 \tag{20}$$

For $\xi = 0$, the hoop fibres does not provide any contribution to strength. The proportioning factor ξ can also be expressed as

$$\xi = \beta_H / \beta_L = E_{2t}^{cs} / E_{1t}^{cs} \tag{21}$$

The thickness of the carbon fibres is assumed as $t_L^{cs} = t_H^{cs}$. Substituting Eqs. (21) into Eq. (17) yields

$$t_{es}^{cs} = \beta_L t_L^{cs} \left(n_L + \xi n_H \right) \tag{22}$$

The non-dimensional fibre reinforcement parameter, for which the hoop fibres are considered, is given by

$$\alpha = \frac{n_L t_L^{cs} + n_H t_H^{cs}}{t^s} \tag{23}$$

By rearranging and substituting the above into Eq. (17), the supplanted thickness t_{es}^{cs} of the beam can be expressed in terms of β_L as

$$t_{es}^{cs} = \beta_L \left(\frac{\alpha t^s}{n_L + n_H} \right) \left(n_L + \xi n_H \right) \tag{24}$$

A simplified expression of the equivalent thickness of the fibre is proposed. The thickness of the supplanted area from CFRP to steel can be defined as

$$t_{es}^{cs} = \frac{1}{\alpha_m} \beta \sum_{j=1}^{m} t_j^{cs} \tag{25}$$

where $\beta = E^{cs}/E^{s}$ and α_m is the percentage of the fibre strength efficiency relative to steel expressed as

$$\alpha_m = \frac{0.19\sigma_u^{cs}}{\sigma_y^{s}} \quad \text{for } 0 \le A_h^{cs} \big/ A_l^{cs} \le 3.0 \tag{26}$$

An approximately 19% fibre stress efficiency is determined by computing the proportion of the compressive strength ($\sigma_{c,cured}^{cs}$) of the cured fibres with respect to the dry fibre tensile strength ($\sigma_{t,dry}^{cs}$) in Seica et al. (2006). The values of these stresses are given in Seica et al. (2006). The percentage of the fibre strength efficiency with respect to steel (α_m) given in Eq. (26) is used in Eq. (25). α_m is used to consider the efficiency of the fibres only in compression and has defined limits which are requisite to the use of bi-orientated CFRP sheets in the CHS beam under pure flexure, and is defined as the ratio of the cross-sectional area of hoop carbon fibre layers (A_h^{cs}) relative to longitudinal layers (A_l^{cs}).

6. Design strength curves for CFRP-reinforced steel CHS

6.1 CHS beams under flexure

The proportioning factor (ξ) for the modulus of elasticity of the hoop CFRP in tension is varied in the range of 0.02 to 0.80. The non-dimensional reinforcement factor α takes the values between 0.10 and 0.30. The strength curves are plotted for a range of yield stress applicable to AS 4600 (1998, 2005), AS 4100 (1998) and EC 3 (2005). The modulus of elasticity for the steel is 200000 N/mm^2, whilst the tensile Young's modulus of the longitudinal CFRP is 230000 N/mm^2. The number of CFRP layers (each with a thickness of 0.176 mm) is ranged from 1 to 4.

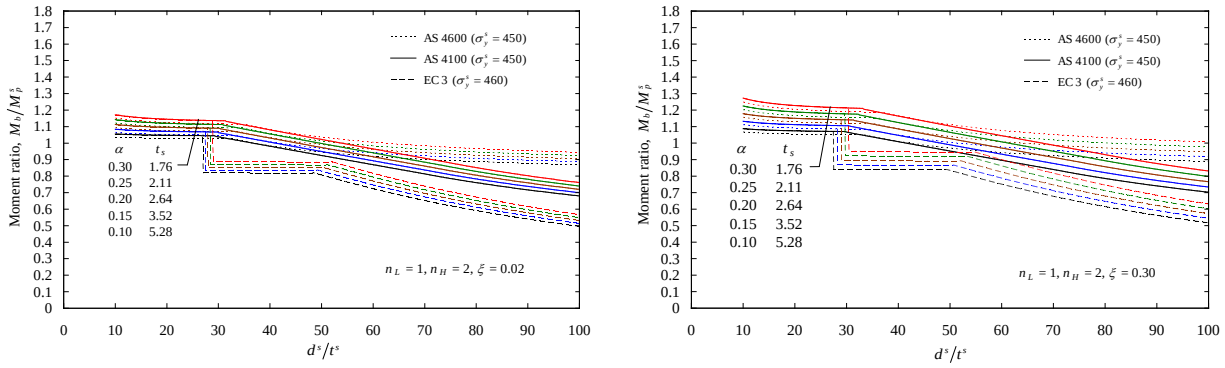

(a) ξ =0.02 (b) ξ = 0.30

Figure 12: Design curves of AS/NZS 4600, AS 4100 and EC 3 for CFRP-reinforced CHS with 2H1L

AS4600, AS4100 and EC3 design curves for strengthened CHS with 2H1L fibre configuration are analysed and shown in Figs. 12(a)-(b). The comparison is given for CHS reinforced with values of ξ = 0.02 and 0.30. As the ξ value increases, it can be seen that the strength increases for increasing values of α.

6.2 Short CHS columns under axial compression

The AS/NZS 4600, AS 4100 and EC 3 non-dimensional strength curves for columns strengthened with 2H2L fibre configurations appear in Figs. 13(a)-(b). The values of ξ used to plot the curves are 0.02 and 0.06. The five values of the reinforcement factor (α = 0.10, 0.15, 0.20, 0.25 and 0.30) delineate the collective design strength curves. The comparison was performed on steel with yield stresses of 450 and 460 N/mm^2 according to the Australian standards and EC 3, respectively. The curves reveal the gain in the strengths of reinforced sections with the increment of the reinforcement factor α. As the α factor changes from 0.25 to 0.30 for 2H2L-reinforced tubes with strength ratios greater than 1.0 and ξ = 0.02-0.06, the AS/NZS 4600 normalized strengths increase by up to 3%, whilst those of AS 4100 and EC 3 gain by 3% and up to 5%, respectively.

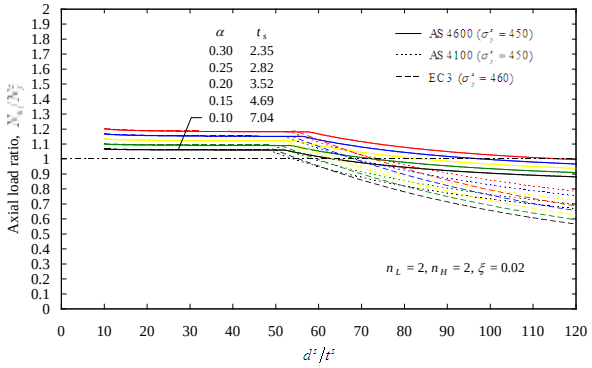

(a) ξ = 0.02 (b) ξ = 0.06

Figure 13: Design curves of AS/NZS 4600, AS 4100 and EC 3 for CFRP-reinforced CHS with 1H

Conclusions

To understand the effects of analysis and design parameters on FRP strengthening of steel structures, one must first understand what the parameters are, and what the available strengthening systems are. The authors have identified key parameters and their relationships with the strengthening system for metallic structures subjected to flexure and axial compression. The beneficial effects of bi-directional FRP strengthening on tubes of wider section slenderness ratios have been reported. It is hoped that this paper will provide a basis for the engineer to approach the problem of selection of a suitable strengthening system for tubular structures.

Acknowledgments

The authors gratefully acknowledge the support of the Australian Research Council for funding a project on FRP strengthening of steel tubular structural systems, and the valuable assistance of the staff at the Monash University Structures Laboratory.

References

Bambach, M.R., Elchalakani, M. (2007). "Plastic mechanism analysis of steel SHS strengthened with CFRP under large axial deformation." *Thin-Walled Structures*, 45 (2) 159-170.

Bambach, M.R., Jama, H.H., Elchalakani, M. (2009). "Axial capacity and design of Thin-Walled steel SHS strengthened with CFRP." *Thin-Walled Structures*, 47 (10) 1112-1121.

Bradford, M.A., Gilbert, R.I. (1989). "Non-linear behaviour of composite beams at service loads." *The Structural Engineer*, 67 (14) 263-268.

Moy, S.S.J. (2001). "*FRP composites: life extension and strengthening of metallic structures, ICE Design and Practice Guides*." Thomas Telford, London, U.K.

Cadei, J.M.C., Stratford, T.J., Hollaway, L.C., Duckett, W.G. (2004). "*Strengthening metallic structures using externally bonded fibre-reinforced composites*." CIRIA, Publication C595, London, U.K.

Colombi, P., Poggi, C. (2006). "An experimental, analytical and numerical study of the static behavior of steel beams reinforced by pultruded CFRP strips." *Composites Part B: Engineering*, 37 (1), 64-73.

Eurocode 3. (2005). "Design of steel structures - Part 1.1: General rules and rules for buildings, EN 1993-1-1:2005." European Committee for Standardisation (CEN), Brussels.

Fawzia, S. (2007). "Bond characteristics between steel and carbon fibre reinforced polymer (CFRP) composites." Ph.D. Thesis, Department of Civil Engineering, Monash University, Melbourne, Australia.

Ghali, A., Favre, R. (1994). Concrete structures - Stresses and deformations, 2nd Edition, E & FN Spon, London.

Haedir, J., Bambach, M.R., Zhao, X.-L., Grzebieta, R.H. (2009). "Strength of circular hollow sections (CHS) tubular beams externally reinforced by carbon FRP sheets in pure bending." *Thin-Walled Structures*, 47 (10) 1136-1147.

Haedir, J., Zhao, X.-L., Bambach, M.R., Grzebieta, R.H. (2010). "Analysis of CFRP externally-reinforced steel CHS tubular beams." *Composite Structures*, 92 (12) 2992-3001.

Haedir, J., Zhao, X.-L. (2010). "Design of short CFRP-reinforced steel tubular columns." *Journal of Constructional Steel Research*, 67 (3) 497-509.

Haedir, J., Zhao, X.-L., Grzebieta, R.H., Bambach, M.R. (2011). "Nonlinear analysis to predict the moment-curvature response of FRP-strengthened steel CHS tubular beams." *Thin-Walled Structures*, 49 (8) 997-1006.

Hollaway, L.C. (2003). "The evolution of and the way forward for advanced polymer composites in the civil infrastructure." *Construction and Building Materials*, 17 (6-7) 365-378.

Hollaway, L.C. (2008). "Advanced fibre polymer composite structural systems used in bridge engineering, ICE manual for bridge engineering." eds, Parkes, G. and Hewson, N., Thomas Telford, London, U.K., 503-529.

Hollaway, L.C. (2010). "A review of the present and future utilisation of FRP composites in the civil infrastructure with reference to their important in-service properties." *Construction and Building Materials*, 24 (12) 2419-2445.

Hollaway, L.C., Cadei, J. (2002). "Progress in the technique of upgrading metallic structures with advanced polymer composites." *Progress in Structural Engineering and Materials*, 4 (2) 131-148.

Hollaway, L.C., Leeming, M.B. (1999). "*Strengthening of reinforced concrete structures*." Woodhead Publishing Limited, Cambridge, England.

Jiao, H., Zhao, X.L. (2004). "CFRP strengthened butt-welded very high strength (VHS) circular steel tubes." *Thin-Walled Structures*, 42 (7) 963-978.

Jones, R.M. (1999). "*Mechanics of composite materials*." Taylor and Francis, Philadelphia.

Kaw, K. (2006). "*Mechanics of composite materials*, CRC Press, Boca Raton

Lanier, B., Schnerch, D., Rizkalla, S. (2009). "Behavior of steel monopoles strengthened with high-modulus CFRP materials." *Thin-Walled Structures*, 47 (10), 1037-1047.

Liu, H., Xiao, Z.G., Zhao, X.-L., Al-Mahaidi, R. (2009). "Prediction of fatigue life for CFRP-strengthened steel plates." *Thin-Walled Structures*, 47 (10) 1069-1077.

Liu, H., Zhao, X.-L., Al-Mahaidi, R. (2010). "Effect of fatigue loading on bond strength between CFRP sheets and steel plates." *International Journal of Structural Stability and Dynamics*, 10 (1) 1-20.

Miller, T.C., Chajes, M.J., Mertz, D.R., Hastings, J.N. (2001). "Strengthening of a steel bridge girder using CFRP plates." *Journal of Bridge Engineering*, 6 (6) 514-522.

Moy, S.S.J., Nikoukar, F. (2002). "Flexural behaviour of steel beams reinforced with carbon fibre reinforced polymer composite." *Proceedings of the International Conference on Advanced Polymer Composites for Structural Applications in Construction (ACIC 2002)*, Southampton, U.K. 195-202.

Nishino, T., Furukawa, T. (2004). "Strength deformation capacities of circular hollow section steel member reinforced with carbon fiber." *Proceedings of the 7th Pacific Structural Steel Conference*, Long Beach, California, U.S.A.

Photiou, N.K., Hollaway, L.C., Chryssanthopoulos, M.K. (2006). "Strengthening of an artificially degraded steel beam utilising a carbon/glass composite system." *Construction and Building Materials*, 20 (1-2) 11-21.

Schnerch, D. (2005). Strengthening of steel structures with high modulus carbon fiber reinforced polymer (CFRP) Materials, *Ph.D. Thesis*, Department of Civil, Construction and Environmental Engineering, North Carolina State University, Raleigh, U.S.A.

Seica, M.V., Packer, J.A. (2007). FRP materials for the rehabilitation of tubular steel structures, for underwater applications, *Composite Structures*, 80(3) 440-450.

Seica, M.V., Packer, J.A., Ramirez, G.P., Bell, S.A.H., Zhao, X.L. (2006). Rehabilitation of tubular members with carbon reinforced polymers, *Proceedings of the 11th International Symposium and IIW International Conference on Tubular Structures*, Québec, Canada, 332-339.

Sen, R., Liby, L., Mullins, G. (2001). "Strengthening steel bridge sections using CFRP laminates." *Composites Part B: Engineering*, 32 (4) 309-322.

Shaat, A., Fam, A. (2004). "Strengthening of short HSS steel columns using FRP sheets." *Proceedings of the 4th International Conference on Advanced Composite Materials in Bridges and Structures (ACMBS IV)*, 20-23 July, Calgary, Canada.

Shaat, A., Fam, A. (2006a). "Axial loading tests on short and long hollow structural steel columns retrofitted using carbon fibre reinforced polymers." *Canadian Journal of Civil Engineering*, 33 (4) 458-470.

Shaat, A., Fam, A. (2006b). "Modeling of axially loaded HSS slender steel members retrofitted with composites." *Proceedings of an International Conference on Advances in Engineering Structures, Mechanics & Construction*, Dordrecht, The Netherlands 227-238.

Shaat, A., Fam, A. (2007). "Fiber-element model for slender HSS columns retrofitted with bonded high-modulus composites" *Journal of Structural Engineering* 133 (1) 85-95.

Shaat, A., Fam, A.Z. (2009). "Slender Steel Columns Strengthened Using High-Modulus CFRP Plates for Buckling Control." *Journal of Composites for Construction*, 13 (1) 2-12.

Standards Australia. (1998). "*AS 4100 Steel structures*." Standards Australia, Sydney.

Standards Australia. (2005). "AS/NZS 4600 *Cold-formed steel structures*." Standards Australia, Sydney.

Standards Australia. (1998). *AS/NZS4600 cold-formed steel structures - commentary (supplement 1 to AS/NZS 4600: 1996)*, Standards Australia, Sydney.

Tavakkolizadeh, M., Saadatmanesh, H. (2003). "Strengthening of steel-concrete composite girders using carbon fibre reinforced polymers sheets." *Journal of Structural Engineering*, 129 (1) 30-40.

Teng, J.G., Chen, J.F., Smith, S.T., Lam, L. (2002). "*FRP strengthened RC structures*." John Wiley & Sons, Chichester, U.K.

Teng, J.G., Hu, Y.M. (2007). "Behaviour of FRP-jacketed circular steel tubes and cylindrical shells under axial compression." *Construction and Building Materials*, 21 (4) 827-838.

Zhao, X.L. (2009). "Thin-walled structure: Special issue--FRP strengthened metallic structures." *Thin-Walled Structures*, 47 (10) 1019.

Zhao, X.L., Hancock, G.J. (1991). "Tests to Determine Plate Slenderness Limits for Cold-Formed Rectangular Hollow Sections of Grade C450." *Journal of Australian Institute of Steel Construction*, 25 (4) 2-16.

Zhao, X.L., Al-Mahaidi, R. (2009). Web buckling of lightsteel beams strengthened with CFRP subjected to end bearing forces." *Thin-Walled Structures*, 47 (10) 1029-1036.

Zhao, X.L., Zhang, L. (2007). "State-of-the-art review on FRP strengthened steel structures." *Engineering Structures*, 29 (8) 1808-1823.

Zhao, X.L., Fernando, D., Al-Mahaidi, R. (2006). "CFRP strengthened RHS subjected to transverse end bearing force." *Engineering Structures*, 28 (11) 1555-1565.

Zhao, X.L., Wilkinson, T., Hancock, G.J. (2005). "*Cold-formed tubular members and connections*." Elsevier, Oxford, U.K.